Journal of Membrane Science 705 (2024) 122850

Contents lists available at ScienceDirect

Journal of Membrane Science

journal homepage: www.elsevier.com/locate/memsci

Characterization of electrokinetic and membrane properties of nanoporous polyimide films via measurements of time-resolved pressure-induced potential

Mykola Bondarenko [a], Stanislaw Koter [b], Andriy Yaroshchuk [c,d,*]

[a] F.D.Ovcharenko Institute of Bio-Colloid Chemistry of National Academy of Sciences of Ukraine, Vernadskiy Ave.42, 03142, Kyiv, Ukraine
[b] Faculty of Chemistry, Nicolaus Copernicus University in Toruń, Gagarin St. 7, 87-100, Toruń, Poland
[c] ICREA, Pg. L.Companys 23, 08010, Barcelona, Spain
[d] Department of Chemical Engineering, Universitat Politècnica de Catalunya, Av. Diagonal 647, 08028, Barcelona, Spain

A B S T R A C T

Charged nanoporous films have interesting ion-separation properties essentially controlled by pore-surface charge density. This (or a related zeta-potential) is often estimated from the so-called streaming potential. However, with nanoporous membranes in sufficiently dilute electrolyte solutions, the pressure-induced electrical response is due not only to streaming potential but also to an electrical response to concentration gradients arising because of a partial salt rejection by charged nanopores. In this study, we refine the methodology of interpretation of measurements of transient filtration potential developed by us previously and apply it to the determination of electrokinetic and membrane properties (in particular, diffusion permeance) of nanoporous polyimide films developed for uses as battery/supercapacitor separators. Diffusion permeance is directly related to electrical conductance, which is an important property of battery/supercapacitor separators.

We observe that in dilute electrolyte solutions (<2 mM KCl), the electrical response to an applied pressure difference is dominated by the concentration potential and not by the classical streaming potential contrary to what is often tacitly assumed. The development of concentration gradients across and around the film takes some time, which enables separate determination of instantaneous (streaming potential) and time-delayed (concentration potential) components. An improved interpretation procedure developed in this study enables estimates of impact of non-linear and osmotic corrections and makes the interpretation more reliable. The results of this study are important for the identification and optimization of novel innovative applications for nanoporous films.

1. Introduction

Charged nanoporous films (membranes) have interesting ion-separation properties, in particular, they can feature strong separations of ions of the same charge but different mobilities in pressure-driven processes [1,2]. They can also be useful for ultralow-pressure ultrapure water production [3,4].

These phenomena are essentially controlled by the pore-surface charge density. This (or related zeta-potential) is often estimated from streaming potential, which is defined as an electric-potential difference induced by an applied pressure difference. However, with nanoporous membranes in sufficiently dilute electrolyte solutions, the pressure-induced electrical response is not only due to streaming potential but also owing to concentration potential arising because of a partial salt rejection by charged nanopores [5–7]. Moreover, in many cases the latter component is even dominant, so its disregard makes correct determination of surface-charge density impossible.

Porous films also routinely serve as separators in batteries, supercapacitors and similar devices [8,9]. Such films must combine high ion conductance with a comprehensive absence of electron conductance. The latter can be compromised, for example in supercapacitors, if during charge/discharge some carbon nanoparticles split off electrode layers and intrude into the separator porous structure eventually forming continuous electron-conducting clusters [10,11]. To better control this, separator materials should have sufficiently small pores to exclude carbon particles sterically and hinder their penetration. Thus, very thin nanoporous films of high porosity are required whose electrical resistance can be difficult to measure directly. Therefore, indirect methods of its determination are of interest. Measurements of transient filtration potential can provide information on the diffusion permeance of thin nanoporous films in electrolyte solutions [7]. This property can be directly related to their electrical resistance.

In this study, we refine the methodology of interpretation of measurements of transient filtration potential developed in Ref. [7] and apply it to the determination of electrokinetic and membrane properties (in particular, diffusion permeance) of nanoporous polyimide (PI) films

* Corresponding author. ICREA, Pg. L.Companys 23, 08010, Barcelona, Spain.
E-mail address: andriy.yaroshchuk@upc.edu (A. Yaroshchuk).

https://doi.org/10.1016/j.memsci.2024.122850
Received 18 March 2024; Received in revised form 2 May 2024; Accepted 5 May 2024
Available online 7 May 2024

developed for uses as battery/supercapacitor separators. Such materials are highly priced for their excellent mechanical strength, thermal stability and chemical inertness [12]. However, membrane and/or electrokinetic properties of nanoporous polyimide films in aqueous electrolyte solutions have not, yet, been studied. The only exception is ref. [13] where streaming potential was measured with a track-etched PI membrane. The smallest pore size was 30 nm and the electrolyte concentration was 10 mM (screening length 3 nm), so salt rejection must have been very low and phenomena investigated in the present study did not occur. Besides, only information on the pore-size dependence of iso-electric point is provided for a PI track-etched membrane in this publication.

Similar to the previously investigated nanoporous track-etched membranes, for PI films we will observe that in dilute solutions (<2 mM KCl), the electrical response to an applied pressure difference is dominated by concentration potential caused by salt-concentration gradients in and around the membrane and not by the classical streaming potential. The concentration gradients arise due to salt rejection by charged nanopores. The development of the gradients takes some time, which enables separate determination of instantaneous (streaming potential) and time-delayed (concentration potential) components.

Previously [7], we developed a simple theoretical model in a linear approximation in the so-called Péclet number and disregarding the effect of osmosis on the transmembrane volume flow. In this study, we will go beyond these approximations and see that for the experimental conditions and materials used, its errors are moderate, so the linear approximation could still provide reasonable initial guesses for the model parameters. At the same time, the use of the full numerical solution brings about (moderate) corrections to model parameters and makes possible approximate separate estimates of those parameters that appear only in combination in the linear approximation. We will conclude that (due to the number of model parameters) additional complementary measurements are needed to make the interpretation still less ambiguous.

2. Theory

2.1. Equations and boundary conditions

Fig. 1 schematically shows the system and the coordinates.

Under zero electric current conditions of this study, ion transfer occurs stoichiometrically, so one can consider the transfer of electroneutral salt. This is described by non-stationary convection diffusion equation. Outside the membrane, it reads this way

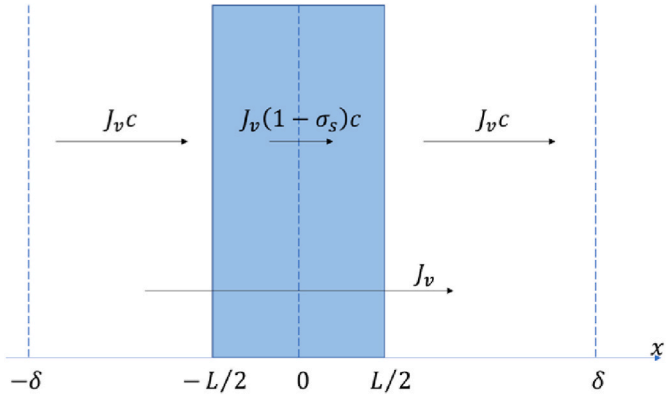

Fig. 1. System schematics and coordinates (not to scale): the upper arrows visualize initial salt fluxes; the flux discontinuities at the membrane surfaces cause salt accumulation close to the left and salt depletion close to the right side of the membrane, $\pm\delta$ denotes boundaries of stagnant layers.

$$\frac{\partial c}{\partial t} = -\frac{\partial J_s}{\partial x} \tag{1}$$

where $c \equiv c(x,t)$ is the position- and time-dependent salt concentration, $J_s \equiv J_s(x,t)$ is the local time-dependent salt flux. It has diffusion and convective components

$$J_s(x,t) = -D\frac{\partial c}{\partial x} + J_v(t)c \tag{2}$$

where D is the salt diffusion coefficient in solution, $J_v(t)$ is the time-dependent *trans*-membrane volume flux, which is position-independent due to the volume conservation in this 1D process.

Inside the membrane, the expression for the salt flux (see the derivation of this expression from the equations for the individual-ion fluxes under zero-current conditions in Ref. [14]) has this form

$$J_{sm}(x,t) = -D_m\frac{\partial c}{\partial x} + J_v(t)(1-\sigma_s)c \tag{3}$$

where σ_s is the salt reflection coefficient, D_m is the salt diffusion coefficient inside the membrane, and c now is the so-called virtual salt concentration defined as the concentration in the solution of the same salt that could be in thermodynamic equilibrium with a given point inside the membrane. According to this definition, this concentration remains continuous at the membrane surfaces (while the real ion concentrations experience quasi-equilibrium "jumps"). Strictly speaking, inside the membrane Eq (1) has to be modified to include the effects of Donnan salt exclusion on the accumulation term in the left-hand side [15]

However, the membrane used in this study is relatively thin and typical measurement times are controlled by processes occurring outside of the membrane and are relatively long. Therefore, one can expect the salt concentration profile inside the membrane to become quasi-stationary (and the salt flux position-independent) after a relatively rapid relaxation. Its characteristic time can be estimated as the square of membrane half-thickness over salt diffusion coefficient. Given the half-thickness of 20 μm and assuming a somewhat reduced (due to pore tortuosity and electrostatic phenomena) diffusion coefficient of $10^{-9}\ m^2/s$, we obtain the characteristic time of 0.4 s. As we will see below, at such short times, the experimental data are rather scattered, thus not really useable for the interpretation. At longer times, one can neglect the time derivative of concentration in Eq (1) (and, thus, disregard the effects of modified chemical capacity inside the membrane), consider the salt flux position-independent across the membrane and solve Eq (3) to obtain

$$J_{sm}(t) = J_v(t)(1-\sigma_s)\bullet\frac{c_{ml}(t)\bullet exp(2Pe(t)(1-\sigma_s)) - c_{mr}(t)}{exp(2Pe(t)(1-\sigma_s)) - 1} \tag{4}$$

where $c_{ml}(t)$ and $c_{mr}(t)$ are (unknown) salt concentrations on the left, and right membrane surfaces, and the dimensionless Péclet number is defined this way

$$Pe(t) \equiv J_v(t)/2P_m \tag{5}$$

$$P_m \equiv \frac{D_m}{L} \tag{6}$$

where P_m is the membrane diffusion permeance to salt, L is the membrane thickness. For the non-stationary-diffusion equation outside the membrane, Eqs(1) and (2), the boundary conditions are:

$$J_s(\pm L/2, t) = J_{sm}(t) \tag{7}$$

salt flux continuity,

$$c(-L/2, t) = c_{ml}(t) \tag{8}$$

virtual-concentration continuity on the feed membrane surface,

$$c(L/2,t) = c_{mr}(t) \tag{9}$$

virtual-concentration continuity on the permeate membrane surface.

Besides, the concentration remains unperturbed far away from the membrane

$$c(\pm\infty,t) = c_0 \tag{10}$$

where c_0 is the initial value of concentration. Although this condition is mathematically set at infinities, in numerical calculations, a finite distance has to be set. In this study, we used the value of 1 mm, which is close to the approximate value of 500 μm suggested in some studies [16] as an effective thickness of stagnant layers in quiescent aqueous solutions experiencing natural convection.

Finally, the initial condition is

$$c(x,0) = c_0 \tag{11}$$

The transmembrane volume flow has pressure-driven and osmotic components according to

$$J_v(t) = A(p(t) - 2RT\sigma_s \bullet (c_{ml}(t) - c_{mr}(t))) \tag{12}$$

where R is the universal gas constant, T is the absolute temperature, and we assume the solution to be ideal (a very good approximation for the concentration range used in this study), A is the membrane hydraulic permeance, $p(t)$ is the time-dependent transmembrane pressure difference. In this study, the pressure difference is applied in a stepwise manner, so

$$p(t) = p_0 H(t) \tag{13}$$

where $H(t)$ is the unit-step function.

Generally, the equation of non-stationary salt diffusion outside the membrane (Eq (1)) coupled to the equation for the volume flow (Eq (12)) and with the complex boundary/initial conditions of Eqs(4), (7)–(11) can be solved only numerically. However, there is an approximate analytical solution discussed in the next section.

2.2. Linear approximation

Deviations of concentration from the initial value are proportional to the membrane Péclet number (and salt reflection coefficient). At not too long times, the concentration changes are localized within relatively narrow zones on two sides of the membrane. Accordingly, diffusion dominates over convection, so the latter can be neglected, and in the solutions outside the membrane, for the evolution of deviations of concentration from the initial value, we obtain classical equation of non-stationary diffusion. The expression for the salt flux (Eq (4)) can also be linearized in Péclet number to obtain:

$$J_{sm} = P_m(c_{ml} - c_{mr}) + J_v c_{ml}(1 - \sigma_s) \tag{14}$$

If we additionally neglect osmosis (this gives rise to a time-independent transmembrane volume flow after the pressure is increased), the resulting linear boundary problem can be solved using Fourier transforms to obtain the following expression for the time evolution of the deviation of concentration from the initial value at the feed (left) membrane surface as a result of a stepwise application of a transmembrane-pressure difference [7]:

$$\frac{c_{ml}(t)}{c_0} - 1 \equiv Pe_0\sigma_s\left[1 - \frac{1}{2\pi}Re\left(\int_{-\infty}^{+\infty} d\omega \frac{exp(i\omega\tau)}{\sqrt{i\omega}(1+\sqrt{i\omega})}\right)\right] \tag{15}$$

where the dimensionless time, τ, is defined this way

$$\tau \equiv t/t_{ch} \tag{16}$$

$$t_{ch} \equiv D/4P_m^2 \tag{17}$$

The integral in the right-hand side of Eq (15) can be taken in terms of a special function. Besides, as the integral depends only on dimensionless time it can be easily tabulated. An approximate analysis of a similar problem (at short dimensionless times) was carried out in Ref. [6] where the term in parenthesis in the right-hand side of Eq (15) was shown to be approximately equal to

$$1 - \frac{1}{2\pi}Re\left(\int_{-\infty}^{+\infty} d\omega \frac{exp(i\omega\tau)}{\sqrt{i\omega}(1+\sqrt{i\omega})}\right) \approx 2\sqrt{\frac{\tau}{\pi}} - \tau \ (\tau \ll 1) \tag{18}$$

A higher-order (and very accurate) polynomial approximation is provided in the Electronic Supporting Information of ref. [7]. Eq (18) shows that it is convenient to plot experimental data as a function of square root of time elapsed after pressure application.

In this linear approximation, the equation is the same in the solutions on both sides of the membrane while the difference between the convective components of the salt flux just outside and just inside the membrane differs only by sign (it is positive on the feed surface and negative on the permeate surface). Therefore, the concentration profiles are anti-symmetrical with respect to the membrane plane of symmetry, and the concentration deviations at two membrane surfaces differ only by sign (see Fig. 2a below). Accordingly, the full concentration difference across the membrane is the double of the difference between the feed surface and the membrane middle.

2.3. Electrical response

As we can see from Fig. 1, there are three zones with concentration gradients in the system: two zones outside the membrane and one inside it. Electrical response to a concentration gradient under zero-current conditions is known to be controlled by ion transport numbers and (in the case of (1:1) electrolytes used in our experiments) can be expressed this way [17–19].

$$\nabla\varphi = \frac{RT}{F}(t_+ - t_-)\nabla ln(c) \equiv \frac{RT}{F}(2t_+ - 1)\frac{\nabla c}{c} \tag{19}$$

Outside the membrane, the ion transport numbers are controlled by bulk ion mobilities. Inside the membrane, there is an additional difference between them due to electrostatic interactions between ions and surface charges. Since the salt concentrations in two reservoirs are equal, the sum of concentration differences across the two diffusion layers is equal in magnitude and opposite in sign to the concentration difference across the membrane, so the sum of all concentration differences is zero. Nevertheless, due to the different ion transport numbers in the membrane and solution, a net electrical response to such situation is non-zero. Assuming that (due to the small deviations of concentration from the equilibrium value) ion transport numbers inside the membrane are independent of concentration (outside the membrane they are reasonably constant anyway), we can integrate Eq (19) within each zone and add up the corresponding voltage differences (with a due account of their signs). As a result, for the full diffusion-related voltage difference across the system (measurable with a pair of reversible electrodes located outside the concentration-polarization layers), we obtain

$$\Delta\varphi_d(t) = \frac{2RT}{F}\left(t_+^{(m)} - t_+^{(b)}\right)ln\left(\frac{c_{ml}(t)}{c_{mr}(t)}\right) \tag{20}$$

where $t_+^{(m)}, t_+^{(b)}$ are the cation transport numbers in the membrane and solution, respectively. The measurable electrical response also contains a streaming-potential component. It arises immediately after pressure switch-on and is proportional to the *trans*-membrane volume flow. The latter somewhat decreases with time due to the buildup of osmotic-pressure difference. The total measurable electric potential difference is

$$\Delta\varphi(t) = \alpha \bullet (p(t) - 2RT\sigma_s \bullet (c_{ml}(t) - c_{mr}(t))) + \frac{2RT}{F}\Delta t_+ \ ln\left(\frac{c_{ml}(t)}{c_{mr}(t)}\right) \tag{21}$$

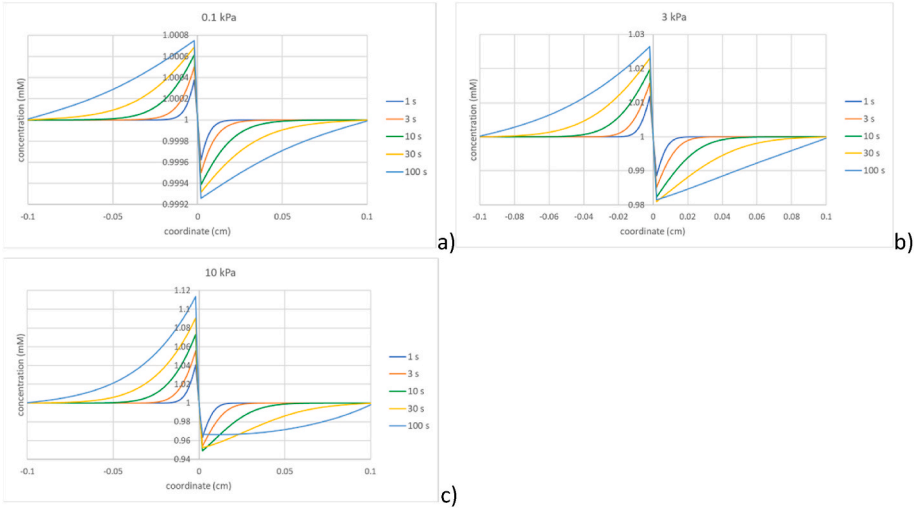

Fig. 2. Salt-concentration profiles calculated numerically for a) linear conditions ($\Delta p_0 = 0.1\ kPa$), b) typical experimental conditions of this study ($\Delta p_0 = 3\ kPa$), c) pronouncedly non-linear conditions ($\Delta p_0 = 10\ kPa$): $A = 5.3 \bullet 10^{-10}\ m/s \bullet Pa$; $P_m = 1.5 \bullet 10^{-5}\ m/s$; $\sigma_s = 0.5$; $c = 1\ mM$; the calculations were performed for $\delta = 1\ mm$.

where α is the streaming-potential coefficient, and we have denoted

$$\Delta t_+ \equiv t_+^{(m)} - t_+^{(b)} \tag{22}$$

Given that in this study, the deviations of salt concentration from the initial value have always been small, the logarithm in Eq (21) can be linearized with respect to the deviation of concentration ratio from unity, and Eq (21) can be transformed to

$$\Delta\varphi(t) \approx \alpha \bullet p(t) + \frac{2RT}{F}(\Delta t_+ - F\alpha\sigma_s c_0)\left(\frac{c_{ml}(t) - c_{mr}(t)}{c_0}\right) \tag{23}$$

Thus, the osmotic correction gives rise to a kind of "renormalization" of difference of cation transport numbers. Eq (23) may be more convenient for interpretation because the first term stays constant (if applied pressure remains constant like in our experiments) while the time-dependent factor in the second term is controlled only by two parameters, namely, salt reflection coefficient and membrane diffusion permeance.

Numerical solutions were obtained using COMSOL Multiphysics software, version 6.1. The number of elements on each side of the membrane was 1000, and the relative tolerance was 0.0002.

3. Experiment

3.1. Membranes

We used nanoporous polyimide films (TAPM-CN1) provided by Tokyo Ohka Kogyo Ltd. Company (Japan). According to the manufacturer, the membrane thickness is 40 μm, the porosity is 70 % and the pores have the shape of 100-nm cavities interconnected by essentially smaller (ca. 20 nm) openings. The average pore size (measured with a porometer) is 30 nm and the pore-size distribution is narrow. This pore shape is due to the process of film fabrication, which consists in mixing silica nanoparticles with a polymer-precursor solution, a thermal treatment ("baking" at 400 °C) and subsequent leaching out of nanoparticles using a HF solution. The procedure of film preparation as well as further information on the membrane properties can be found in Ref. [20]. The membrane structure is symmetrical (the same pore size and structure across the whole thickness), which enables the relatively simple interpretation.

3.2. Setup and measurement procedure

The experimental setup was the same as used in Ref. [7] (see Fig. S1 in the Supporting Information). To measure the potential difference Ag/AgCl electrodes were used; they were connected to a multi-meter with an internal memory; the sampling rate was 0.1 s. A desired pressure difference was obtained by lifting a bottle with the KCl solution connected to one of the cell compartments to an appropriate height above the cell. The exposed membrane area was 1.13 cm^2. The temperature was around 20 °C, KCl solution had pH5.1–5.2. This relatively low pH value occurred for solutions equilibrated with the ambient atmosphere for sufficiently long time. In previous measurements with track-etched membranes, we noticed that pH value of freshly-prepared solutions drifted, which impaired reproducibility of the measurements. Effectively, our working solutions were buffered by CO_2 dissolved from the atmosphere.

The same setup was used for the determination of membrane hydraulic permeance (see Supporting Information).

According to the manufacturer, the studied PI films are slightly hydrophobic. To facilitate wetting by aqueous solutions, samples were pre-wetted by 96 % ethanol (for two days), then transferred to 1 mM KCl. Before the measurements, the samples were equilibrated with a given KCl solution for one day.

As one can see, for example, from Fig. 4b below, some non-zero signals at zero pressure difference occurred (probably, due to a potential of asymmetry of the electrodes). Moreover, this potential difference slowly drifted with time slightly changing from one individual measurement to another. To take this into account and obtain a genuine pressure-induced potential, the signal was averaged over 5 s preceding each pressure application, and the corresponding value was subtracted from the measured signal. Thus, we supposed the drift to be negligible at the time scale of the relatively short pressure-induced runs although actually it could give rise to some additional data scattering at the end of the runs (see Fig. 5).

4. Results and discussion

Fig. 2 shows the profiles of salt concentration (virtual salt concentration inside the membrane) calculated numerically using Eqs 1–13. The profiles in Fig. 2a are practically identical to the linear approximation due to the very low pressure. True, in contrast to the linear approximation, the calculations shown in Fig. 2a include the osmotic

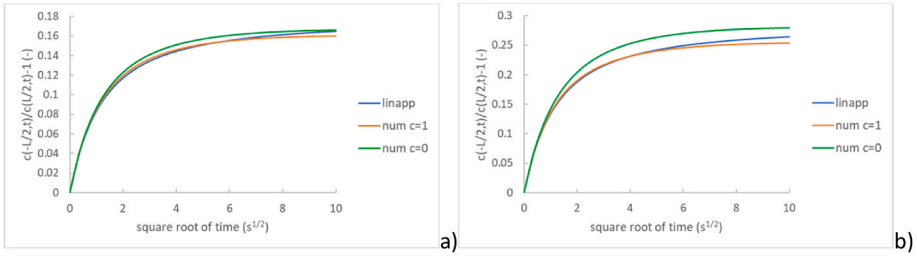

Fig. 3. Time dependencies of deviation of ratio of concentrations on the membrane surfaces from the initial value: $p = 10\ kPa$; $A = 5.3 \bullet 10^{-10}\ m/s \bullet Pa$; $P_m = 1.5 \bullet 10^{-5}\ m/s$; $\sigma_s = 0.5$ (a); $\sigma_s = 0.8$ (b); the blue lines show the results obtained in the linear approximation (linapp); num c = 1 and num c = 0 denote numerical solutions obtained for a finite (1 mM) and an infinitely low concentration (no osmosis), respectively.

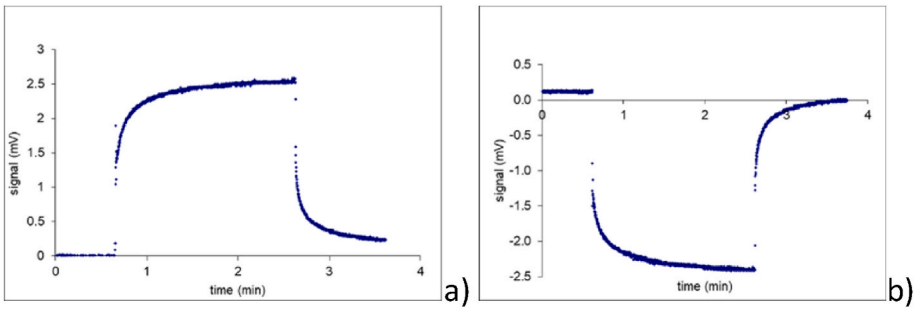

Fig. 4. Examples of "raw" data: $\Delta p_0 = 4.4\ kPa$, $c_0 = 0.5\ mM\ KCl$.

correction given by Eq (12). However, this only slightly modifies the transmembrane volume flow while the nonlinear convective corrections remain negligible due to very small Péclet numbers. Accordingly, the profiles on both sides of the membrane remain strictly anti-symmetrical. At higher pressures, this feature is approximately preserved at very short times but is progressively lost at longer times.

Nevertheless, on the high-pressure side, the profiles don't change qualitatively, they just become more non-linear. On the low-pressure side, at longer times, they change shape qualitatively turning from concave up to concave down. Fig. 2 also shows that the intrinsic salt rejection (the ratio of concentrations on the left and right sides of the membrane minus one) expectedly increases with time but always remains quite small, namely, in the range of single percentage points (at $p_0 = 3\ kPa$). The same was true in our experiments and made applicable our assumption of constant coefficients.

Although concentration profiles differ considerably (and even qualitatively) from the linear approximation, the time dependencies of the deviation of the ratio of concentrations at the membrane surfaces from unity (indirectly observable experimentally via the electrical response) remain qualitatively similar to it. This is illustrated by Fig. 3.

As we can see, in very dilute solutions ($c = 0$), non-linear phenomena can make the effect somewhat stronger than in the linear approximation although the relaxation is also a bit faster, so the difference decreases with time. On the other hand, osmosis brings about smaller concentration-ratio deviations because it reduces transmembrane volume flow. As a result, non-linear and osmotic corrections can partially compensate each other giving rise to a better overall applicability of the linear approximation (see Fig. 3b). However, the extent of this error compensation depends on the system parameters and cannot be considered a general feature. Fig. 3 also shows that the impact of osmotic corrections rather strongly depends on the salt reflection coefficient. This occurs because the transmembrane concentration difference is proportional to this coefficient while the osmotic counterflow (at a given concentration difference) is proportional to it, too. This results in an approximately quadratic dependence.

Fig. 4 shows examples of "raw" experimental data directly measured by the data-acquisition system. Fig. 4b) shows the signal recorded when pressure was applied from the opposite side of the membrane than in Fig. 4a). One can see that the signal just changed sign, which illustrates that the membrane was symmetrical. This was also confirmed in a more rigorous way via separate statistical analysis of signals obtained with two membrane orientations: no significant difference was observed within experimental errors.

Fig. 4 shows that we also recorded signal after pressure switch-offs (primarily, to monitor approaching the initial state prior to the subsequent measurement). The corresponding signal relaxation is of potential use for the membrane characterization (as described, for example, in Ref. [21]). However, to make use of such data, the initial state prior to the switch-off has to be properly defined. In our test cell without stirring, this is difficult due to the poorly defined thickness of stagnant layer. Therefore, for the interpretation, we used only data obtained after pressure switch-on.

Fig. 5 shows the experimental data plotted vs. square root of time elapsed from the moment of pressure application. In our measurements, the time step was 0.1 s, and Fig. 4 shows that the signal initially changed very quickly within a couple of time steps. These initial very rapid changes are due to the buildup of streaming potential, which takes some time because of non-instantaneous valve opening as well as other poorly controllable factors. The switch-on time was defined as the first datapoint where the signal deviated by >10 % of the full signal variation from the previous (almost constant) value. With this definition of starting time, the data shown in Fig. 5 at very short times could sometimes be affected by an incomplete buildup of streaming potential. This probably caused the relatively poor data reproducibility at very short times < 1s. At longer times, the reproducibility is quite good even in the most concentrated solution (2 mM) where the signal magnitude is quite small (<1 mV). As discussed above, the somewhat stronger scattering at longer times may be due to some electrode instability.

In contrast to the previously studied track-etched membranes [7](or even more so in the case of ion-exchange membranes investigated in Ref. [6]), for the PI films the characteristic relaxation times are too short to make possible an effective use of the initial linear parts of dependences of signal on the square root of time for the determination of the initial slope and intersect (streaming potential). Indeed, Fig. 6 shows

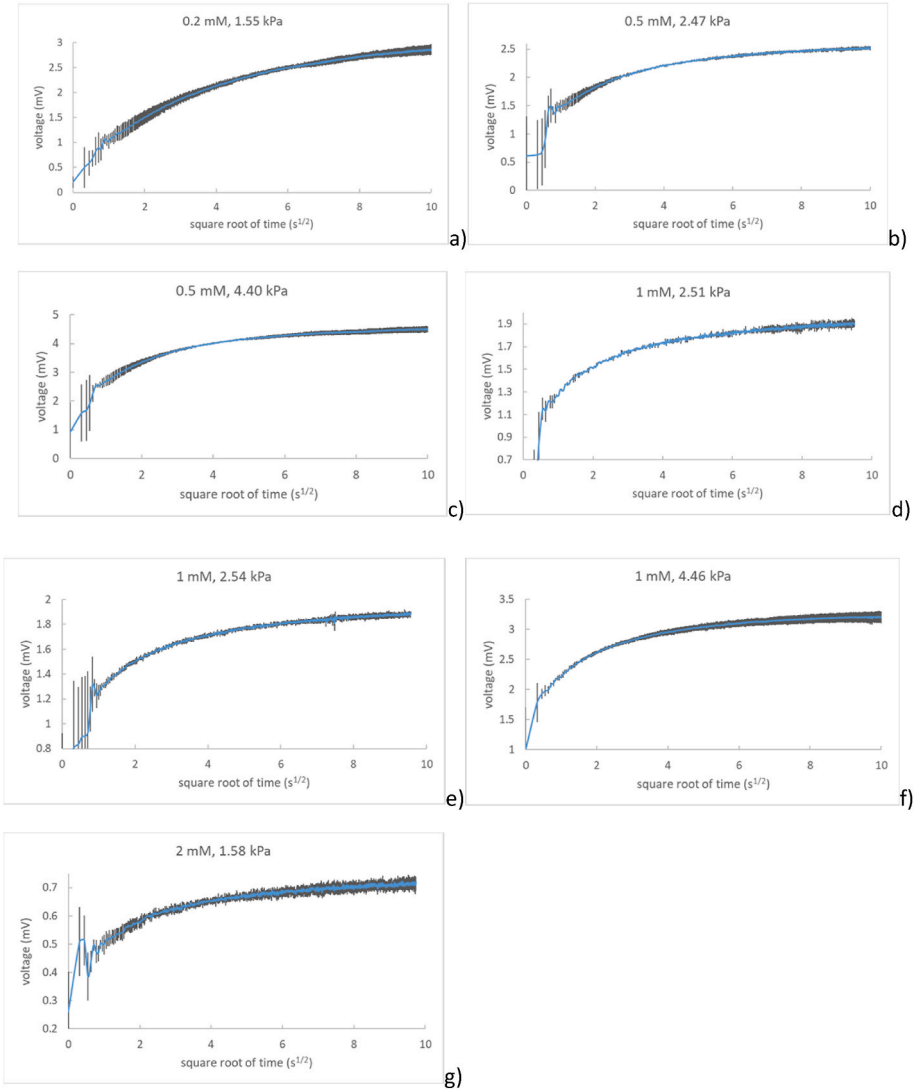

Fig. 5. Electrical response to step-wise pressure application vs. square root of time elapsed after it. Solution concentrations and applied pressures are indicated in the chart titles. Each set of data is an average of 4–8 repeated measurements.

that the theoretical curves are linear only at quite short times where the experimental data are too scattered. This in agreement with the fact that according to the values of diffusion permeance listed in Table 1 below and the definition of characteristic relaxation time of Eq (17), the latter was just around 3–4 s while according to Eq (18) a good initial linearity (<5–7% deviations from linearity) occurs only for dimensionless times $\tau < 0.1$ that is for dimensional times less than 0.3–0.4 s.

Nevertheless, the three parameters, which control the time dependences in the linear approximation can be fitted in a unique way. Indeed, the product of salt reflection coefficient and difference of cation transport numbers controls the overall signal magnitude while the characteristic relaxation time (controlled by the diffusion permeance) controls the extent of deviations from the initial linearity. The curve extension to very short times gives the value of streaming potential.

The red curves in Fig. 6 simultaneously show theoretical fits obtained in two ways: using the linear approximation and the numerical solution (with adjusted values of parameters, see below). These curves are so close to each other that they cannot be distinguished in the graphs. In the linear approximation, three model parameters could be fitted. However, the numerical solution explicitly depends on four separate parameters because the salt reflection coefficient controls not only the signal magnitude but also the osmotic corrections to the transmembrane volume flow (see Eq (12)). Simultaneous unambiguous determination of four parameters is very difficult. Therefore, in the fitting by the numerical solution, we had to fix one of the four parameters. We assumed that the difference of cation transport numbers was equal to its maximum possible value of 0.5. The green curves in Fig. 6 show dependencies calculated using the numerical solution and the values of parameters fitted to the linear approximation (and assuming additionally $\Delta t_+ = 0.5$). Thus, the deviations of the green curves from the red ones (and the experimental data) illustrate the extent of interpretation error due to the use of linear approximation. These deviations are rather moderate. As already mentioned, the red curves also show fits obtained using the numerical solution. The excellent agreement of the numerical solution with the experimental data could be restored by adjusting just one parameter, namely, membrane diffusion permeance. Table 1 shows that the corresponding adjustments are quite moderate (<10 %), too.

To evaluate the applicability of the assumption of ideal membrane perm-selectivity, we performed measurements of stationary membrane potential in a stirred cell (see Supporting Information, Section 2. Measurements of stationary membrane potential) for solutions of 2 mM and 1 mM KCl separated by the membrane. Their interpretation in terms of ion perm-selectivity of the membrane is complicated by the very high membrane diffusion permeance, which makes the contribution of unstirred layers quite significant. On the other hand, the thickness of such layers in test cells agitated by magnetic stirrers (especially, those

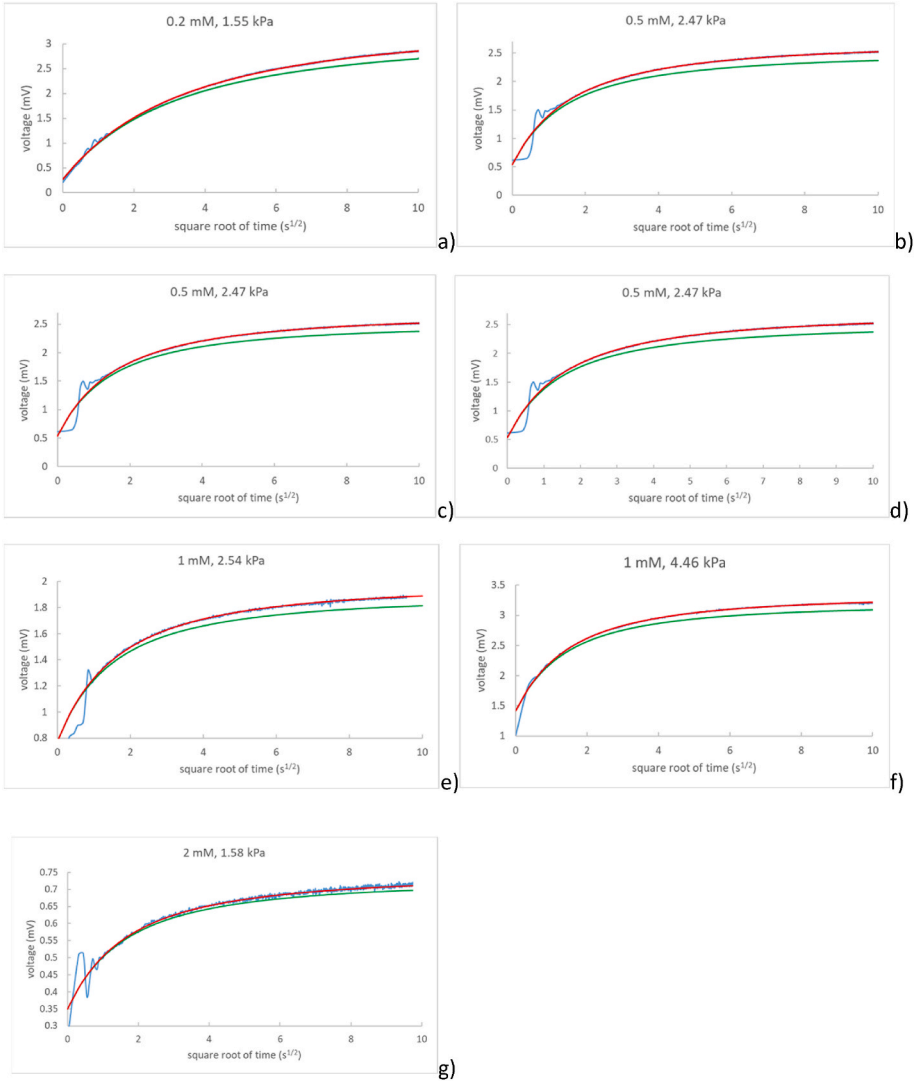

Fig. 6. Experimental data (blue) and their fits by the model (red and green). Solution concentrations and applied pressures are indicated in the chart titles. Explanations of the fitting procedures are in the text.

Table 1
Parameters obtained as a result of fitting the model to experimental data.

conc. (mM)	pressure (kPa)	SP coef. (μV/kPa)	$\sigma_s \Delta t_+$	σ_s	P_m ($\mu m/s$) linear	P_m ($\mu m/s$) numerical
0.2	1.55	−174	0.42	0.84	5.45	5.00
0.5	2.47	−217	0.38	0.76	11.6	10.6
0.5	4.40	−205	0.44	0.89	13.5	12.0
1.0	2.51	−305	0.27	0.54	15.3	14.5
1.0	2.54	−305	0.21	0.41	11.6	10.7
1.0	4.46	−318	0.20	0.41	12.4	11.4
2.0	1.58	−221	0.11	0.21	11.1	10.6

located at the cell bottom) is poorly known. Nonetheless, assuming a characteristic value of 100 μm for this thickness, and the membrane diffusion permeance of 12 μm/s (the average of the values obtained via numerical fitting for the concentrations of 1 mM and 2 mM), for the ideal membrane perm-selectivity we obtain a stationary membrane plus electrode potential (measured with bare Ag/AgCl electrodes) of 25.0 mV (see Supporting Information, Section 2. Measurements of stationary membrane potential) while around 24.4 ± 0.4 mV (averaged over 6 repeated measurements) was actually measured. Thus, the assumption of ideal perm-selectivity ($\Delta t_+ = 0.5$) can be quite close to reality even for the more concentrated solutions of those used in this study. In more dilute solutions, this assumption would be even more realistic because electrostatic exclusion of coions (leading to ideal perm-selectivity) gets stronger with dilution. Of course, it cannot be excluded that unstirred layers were actually thinner. More reliable estimates of membrane perm-selectivity will be attempted in future studies via measurements of transient membrane potential after concentration step [15,18].

5. Discussion of concentration dependencies

At concentration-independent surface-charge density, SP coefficient should increase (in absolute value) with decreasing concentration in monotone way [22] reaching saturation. Table 1 shows that actually its concentration dependence features a maximum, which can be explained by a surface-charge density decreasing with decreasing electrolyte concentration. Such trend has previously been observed, for example, for track-etched membranes [7] and is typical for dissociation of weakly-acidic (or -basic) ionogenic groups [23].

Salt reflection coefficient is essentially controlled by the exclusion of coions from central parts of pores where the velocity of pressure-driven flow is the largest. Therefore, this parameter is especially sensitive to the extent of overlap of diffuse parts of EDLs and can be expected to increase (approaching unity) with decreasing concentration. This trend can be

partially counteracted by the surface-charge density decreasing in more dilute solutions. Indeed, in 0.2 mM solution this coefficient is only marginally larger than (the average value) in 0.5 mM solution although with the same surface-charge density one could expect a considerable increase due to the 60 % larger screening length (and, thus, a much better EDL overlap) in the 0.2 mM solution.

Due to coion-exclusion phenomena, salt diffusion permeance can be expected to be an increasing function of concentration. This can be modified by a dependence of surface-charge density on concentration. Besides, it was demonstrated theoretically [24] that in not too small (compared to the screening length) charged nanopores salt permeability can be a non-monotone function of salt concentration. The concentration dependence with a broad maximum could be a consequence of these factors as well as of the particular pore geometry of this membrane. To achieve more clarity, additional measurements (for example, transient membrane potential after concentration step [15,18]) will be carried out in future studies. They can provide additional information on the ion transport numbers in the membrane and its diffusion permeance.

6. Conclusions

The methodology of time-resolved measurements of filtration potential after stepwise application of *trans*-membrane pressure difference has been refined to include in the interpretation non-linear and osmotic phenomena and has been used for the characterization of membrane properties of nanoporous polyimide films originally developed as battery separators. Along with streaming-potential coefficient, salt reflection coefficient and diffusion permeance could be (approximately) determined from the data analysis. Diffusion permeance is directly related to the electrical resistance, which is an important property of battery separators but is difficult to measure directly for thin and highly-porous films.

Although in this study the previously developed linear approximation provided a reasonably good fit quality, extensions towards higher pressures and/or smaller nanopores will require a direct use of the full numerical solution. This is controlled by four model parameters whose unambiguous determination from fitting single time dependences is very difficult. Therefore, in future studies, complementary measurements (for example, transient membrane potential after concentration step [15,18]) will have to be used for unambiguous determination of model parameters. A mechanistic interpretation within the scope of space-charge model (taking into account the pore geometry of this material) will also be attempted to make possible determination of surface-charge density.

As discussed in Ref. [7], the methodology of this study (especially, the interpretation procedure) is essentially limited to monolayer membranes. Other transient electrical methods (for example, concentration step [18] or pressure switch-off [25]) are available for the characterization of electrochemical perm-selectivity of active layers of composite/asymmetric membranes.

CRediT authorship contribution statement

Mykola Bondarenko: Software, Methodology. **Stanislaw Koter:** Writing – review & editing, Methodology, Investigation, Conceptualization. **Andriy Yaroshchuk:** Writing – review & editing, Writing – original draft, Methodology, Investigation, Conceptualization.

Declaration of competing interest

The authors declare no conflict of interests.

Data availability

Data will be made available on request.

Acknowledgements

Tokyo Ohka Kogyo (TOK) Company is acknowledged for the supply of the samples of nanoporous PI films. The authors are grateful to T. Yokoyama (New Business Development Dept. Of TOK) for information on the film properties. A.Y. and M.B. acknowledge funding from the European Union through Project H2020-FETOPEN-2018-2019-2020-01-964524 “Energy harvesting via wetting/drying cycles with nanoporous electrodes (EHAWEDRY)”. S.K. thanks for the funds for fundamental research from Nicolaus Copernicus University in Torun, Poland (Faculty of Chemistry – “Membranes and membrane separation processes - fundamental and applied research”).

Appendix A. Supplementary data

Supplementary data to this article can be found online at https://doi.org/10.1016/j.memsci.2024.122850.

References

[1] C. Tang, A. Yaroshchuk, M.L. Bruening, Ion separations based on spontaneously arising streaming potentials in rotating isoporous membranes, Membranes 12 (2022) 631, https://doi.org/10.3390/MEMBRANES12060631.
[2] C. Tang, A. Yaroshchuk, M.L. Bruening, Flow through negatively charged, nanoporous membranes separates Li+and K+due to induced electromigration, Chem. Commun. 56 (2020) 10954–10957, https://doi.org/10.1039/d0cc03143g.
[3] Andriy Yaroshchuk, Transport properties of nano-porous track-etched membranes in electrolyte solutions, in: J.B. Edel, T. Albrecht (Eds.), Nanopores for Bioanalytical Applications: Proceedings of the First International Conference, Lanzarote, Spain, February 6-10, 2012, RSC Publishing, 2012, pp. 93–99.
[4] A. Yaroshchuk, E. Staude, Charged membranes for low pressure reverse osmosis properties and applications, Desalination 86 (1992) 115–133, https://doi.org/10.1016/0011-9164(92)80029-9.
[5] E. Brendler, S. Kjelstrup Ratkje, H.G. Hertz, Streaming potentials of Nucleopore membranes by the electric work method, Electrochim. Acta 41 (1996) 169–176.
[6] T. Okada, S. Kjelstrup Ratkje, H. Hanche-Olsen, Water transport in cation exchange membranes, J. Membr. Sci. 66 (1992) 179–192, https://doi.org/10.1016/0376-7388(92)87008-L.
[7] P. Apel, S. Koter, A. Yaroshchuk, Time-resolved pressure-induced electric potential in nanoporous membranes: measurement and mechanistic interpretation, J. Membr. Sci. 653 (2022) 120556, https://doi.org/10.1016/J.MEMSCI.2022.120556.
[8] N. Lingappan, W. Lee, S. Passerini, M. Pecht, A comprehensive review of separator membranes in lithium-ion batteries, Renew. Sustain. Energy Rev. 187 (2023), https://doi.org/10.1016/J.RSER.2023.113726.
[9] W. Dong, M. Xie, S. Zhao, Q. Qin, F. Huang, Materials design and preparation for high energy density and high power density electrochemical supercapacitors, Mater. Sci. Eng. R Rep. 152 (2023), https://doi.org/10.1016/J.MSER.2022.100713.
[10] K. Liu, C. Yu, W. Guo, L. Ni, J. Yu, Y. Xie, Z. Wang, Y. Ren, J. Qiu, Recent research advances of self-discharge in supercapacitors: mechanisms and suppressing strategies, J. Energy Chem. 58 (2021) 94–109, https://doi.org/10.1016/J.JECHEM.2020.09.041.
[11] Q. Wu, T. He, Y. Zhang, J. Zhang, Z. Wang, Y. Liu, L. Zhao, Y. Wu, F. Ran, Cyclic stability of supercapacitors: materials, energy storage mechanism, test methods, and device, J Mater Chem A Mater 9 (2021) 24094–24147, https://doi.org/10.1039/D1TA06815F.
[12] M. Zhang, L. Wang, H. Xu, Y. Song, X. He, Polyimides as promising materials for lithium-ion batteries: a review, Nano-Micro Lett. 15 (2023), https://doi.org/10.1007/S40820-023-01104-7.
[13] A.I. Vilensky, V.V. Berezkin, V.D. Sobolev, K.G. Sabbatovsky, Y.K. Kochnev, S. V. Vlasov, B.V. McHedlishvili, Electrokinetic study of etching latent tracks of accelerated heavy ions in poly(ethylene terephthalate) and polyimide, Colloid J. 71 (2009) 470–473, https://doi.org/10.1134/S1061933X09040061.
[14] A. Yaroshchuk, M.L. Bruening, E. Zholkovskiy, Modelling nanofiltration of electrolyte solutions, Adv. Colloid Interface Sci. 268 (2019) 39–63, https://doi.org/10.1016/j.cis.2019.03.004.
[15] M. Fernández de Labastida, A. Yaroshchuk, Transient membrane potential after concentration step: a new method for advanced characterization of ion-exchange membranes, J. Membr. Sci. 585 (2019) 271–281, https://doi.org/10.1016/j.memsci.2019.05.012.
[16] C. Amatore, S. Szunerits, L. Thouin, J.-S. Warkocz, The real meaning of Nernst’s steady diffusion layer concept under non-forced hydrodynamic conditions. A simple model based on Levich’s seminal view of convection, J. Electroanal. Chem. 500 (2001) 62–70, https://doi.org/10.1016/S0022-0728(00)00378-8.
[17] A. Yaroshchuk, O. Zhukova, M. Ulbricht, V. Ribitsch, Electrochemical and Other Transport Properties of Nanoporous Track-Etched Membranes Studied by the Current Switch-Off Technique, Langmuir 21 (n.d.) 6872–6882. https://doi.org/10.1021/la050499g..

[18] A. Yaroshchuk, Y. Boiko, A. Makovetskiy, Electrochemical perm-selectivity of active layers and diffusion permeability of supports of an asymmetric and a composite NF membrane studied by concentration-step method, Desalination 245 (2009) 374–387, https://doi.org/10.1016/j.desal.2009.02.001.
[19] A. Yaroshchuk, Y. Boiko, A. Makovetskiy, Ion-Rejection, Electrokinetic and Electrochemical Properties of a Nanoporous Track-Etched Membrane and Their Interpretation by Means of Space Charge Model, Langmuir 25 (n.d.) 9605–9614. https://doi.org/10.1021/la900737q..
[20] T. Sugawara, J. Koshiyama, A. Kawai, Novel fabrication of three-dimensional homogeneous microporous polyimide membrane, J. Photopolym. Sci. Technol. 31 (2018) 437–440.
[21] A. Yaroshchuk, Y. Boiko, A. Makovetskiy, Some Properties of Electrolyte Solutions in Nanoconfinement Revealed by the Measurement of Transient Filtration Potential after Pressure Switch Off, Langmuir 21 (n.d.) 7680–7690. https://doi.org/10.1021/la050917h..
[22] A.E. Yaroshchuk, S.S. Dukhin, Phenomenological theory of reverse osmosis in macroscopically homogeneous membranes and its specification for the capillary space-charge model, J. Membr. Sci. 79 (1993), https://doi.org/10.1016/0376-7388(93)85113-B.
[23] R.J. Hunter, Zeta Potential in Colloid Science: Principles and Applications, 1981.
[24] A.E. Yaroshchuk, Transport properties of long straight nano-channels in electrolyte solutions: a systematic approach, Adv. Colloid Interface Sci. 168 (2011) 278–291, https://doi.org/10.1016/j.cis.2011.03.009.
[25] A.E. Yaroshchuk, Y.P. Boiko, A.L. Makovetskiy, Some properties of electrolyte solutions in nanoconfinement revealed by the measurement of transient filtration potential after pressure switch off, Langmuir 21 (2005) 7680–7690, https://doi.org/10.1021/la050917h.